Published in final edited form as:
IEEE Trans Med Imaging. 2012 July ; 31(7): 1337–1345. doi:10.1109/TMI.2011.2182618.

Alignment of 3-D Optical Coherence Tomography Scans to Correct Eye Movement Using a Particle Filtering

Juan Xu[*] **[Member, IEEE]**,
Department of Ophthalmology, UPMC Eye Center, University of Pittsburgh School of Medicine, Pittsburgh, PA 15213 USA

Hiroshi Ishikawa,
Department of Ophthalmology, UPMC Eye Center, University of Pittsburgh School of Medicine, Pittsburgh, PA 15213 USA (ishikawah@upmc.edu)

Gadi Wollstein,
Department of Ophthalmology, UPMC Eye Center, University of Pittsburgh School of Medicine, Pittsburgh, PA 15213 USA (wollsteing@upmc.edu)

Larry Kagemann, and
Department of Bioengineering, Swanson School of Engineering, University of Pittsburgh, Pittsburgh, PA 15213 USA (kagemannl@upmc.edu)

Joel S. Schuman
Department of Bioengineering, Swanson School of Engineering, University of Pittsburgh, Pittsburgh, PA 15213 USA (schumanJS@upmc.edu)

Abstract

Eye movement artifacts occurring during 3-D optical coherence tomography (OCT) scanning is a well-recognized problem that may adversely affect image analysis and interpretation. A particle filtering algorithm is presented in this paper to correct motion in a 3-D dataset by considering eye movement as a target tracking problem in a dynamic system. The proposed particle filtering algorithm is an independent 3-D alignment approach, which does not rely on any reference image. 3-D OCT data is considered as a dynamic system, while the location of each A-scan is represented by the state space. A particle set is used to approximate the probability density of the state in the dynamic system. The state of the system is updated frame by frame to detect A-scan movement. The proposed method was applied on both simulated data for objective evaluation and experimental data for subjective evaluation. The sensitivity and specificity of the x-movement detection were 98.85% and 99.43%, respectively, in the simulated data. For the experimental data (74 3-D OCT images), all the images were improved after z-alignment, while 81.1% images were improved after x-alignment. The proposed algorithm is an efficient way to align 3-D OCT volume data and correct the eye movement without using references.

Keywords

Eye movement correction; particle filtering; retinal image processing; three-dimensional optical coherence tomography (3-D OCT)

[*](xxujuan@gmail.com). .

I. INTRODUCTION

SPECTRAL domain optical coherence tomography (SD-OCT) is a high-speed, high-resolution imaging technology that has gained a significant clinical impact in ophthalmology [1]. Eye movement during 3-D SD-OCT imaging has been recognized as an important problem in OCT structural assessment of various eye diseases. An ideal 3-D OCT volume data is illustrated in Fig. 1(a), which is composed of a series of cross-sectional scans (B-scan) from top to bottom (in the x-y plane) of the scanning region on retina [Fig. 1(b)]. Each B-scan consists of multiple high-resolution 1-D scans in the z direction (A-scan). A typical scan protocol has a fast scan axis in the x direction [Fig. 1(a)]. Eye movement during 3-D SD-OCT scanning, however, creates significant spatial distortions in the 3-D data that may adversely affect qualitative image interpretation and quantitative analysis [Fig. 1(c)]. Obtaining spatial integrity restored (nondistorted) 3-D OCT data is the essential foundation of reliable and reproducible quantitative OCT measurements, which is particularly important in assessing disease longitudinally.

Movement during scanning is a common problem in 3-D medical imaging, e.g., eye movement in OCT imaging or head movement in brain magnetic resonance imaging (MRI) or positron emission tomography (PET) imaging. Strategies for correcting movement can be grouped into two main categories: device-based method (hardware solution) and image-based method (software solution). The device-based method is usually involves real-time processing, which uses a device to monitor the subject movement during data acquisition. The movement information, such as orientation and displacement, detected by the device is used to align the frame image using corresponding software [2]–[4]. The image-based method is solely based on the image data. The typical method involves registering one or multiple misaligned frame images to a reference position, such as the first frame image or additional reference image/scan [5], [6]. The kernel of image registration is to optimize a cost-function generated from a transformation model (movement model) and similarity measurements between two images [7], [8]. The two registered images are generally assumed as static images globally or locally, while the transformation models commonly used are the rigid model, affine model, piecewise affine model, and nonrigid model [9]. An important step in the transformation model includes extracting common features from two images to compute the cost-function in image registration method.

Compared to subject movement problems in other 3-D imaging devices, 3-D OCT eye movement correction is a challenging problem due to the following.

- The complicated nature of eye movement makes it difficult to design a uniform transformation model for the entire 3-D dataset. For example, micro-saccades cause local discontinuities likely generating inter-B-scan movement [x-axis movement, Fig. 1(d)]. Drifts are slow and continuous movements causing stretching/shrinking in 3-D volume data in all directions likely generating intra-B-scan movement. The fore–aft eye movement generates z-axis movement [Fig. 1(e)].
- Due to the fore–aft eye movement, a B-scan cannot be considered as a static image. There is a variable amount of z-axis movement for each A-scan within a B-scan.
- Common 2-D features in the frame image are not reliable due to intra-B-scan movement and these features are fundamental to image registration.

Some hardware solutions were made by the OCT manufactures to resolve some of the eye movement problems. Spectralis HRA-OCT (Heidelberg Engineering, Heidelberg, Germany) uses a real time eye motion tracking system to track eye movement, guide OCT to the proper location, and repeat the B-scan if there was eye movement detected during scanning [10]. The tracking system is an effective solution for x- and y-axis movements, while z-alignment

still requires a software correction. Another hardware solution approach employed by Cirrus HD-OCT (Carl Zeiss Meditec, Dublin, CA) acquires two diagonal B-scans in addition to the 3-D raster scans that are mainly used for z-offset correction [11].

A few publications addressed image-based correction methods in 3-D OCT volume data. Ricco *et al.* [7] proposed a local image registration algorithm to correct x- and y-axis eye movement. A 2-D OCT fundus image [generated by averaging each A-scan, Fig. 1(d)] was locally registered on a static reference image using an affine transformation model. Xu *et al.* [8] introduced another global image registration approach based on the shape context algorithm [12] in order to correct x- and y-axis movements. Retinal blood vessels were detected on the 3-D OCT image [13] and static reference image [14]. A vessel map was then globally registered between the two images using a 2-D deformable model computed by the vessel shape context. However, since the reference image is a 2-D image in the x- and y-plane, fore–aft eye movement in the z direction is not accounted for by these two methods. Kraus *et al.* [15] introduced another method, which combined multiple 3-D OCT scans into one 3-D OCT volume data to compensate for motion in all three dimensions. A global cost-function was optimized to estimate two dense displacement fields that were used for modeling the object motion during the scans. At least two consecutive 3-D OCT scans with orthogonal fast scan axes are required in this method. Antony *et al.* [16] proposed a segmentation-based method for the correction of axial artifacts. The retinal layer segmentation result was used to generate a reference plane based on thin-plate spline technique. The 3-D OCT data was aligned with the reference plane to correct the distortions. All the previous studies either relied on other processing, such as retinal layer segmentation, or used additional reference images or scans to correct the 3-D OCT image. However, not all OCT devices provide additional B-scans or a 2-D reference image to be used by the software correction. Therefore, eye movements occurring during OCT scanning remains a fundamental problem that needs to be solved.

We introduce herein a new method to present a static 3-D dataset using a dynamic system, where the eye movement correction problem is handled as an object tracking problem in the dynamic system. A particle filtering algorithm is proposed to automatically align A-scans and correct x- and z-axis eye movement artifacts in 3-D SD-OCT images. The current 3-D OCT scan pattern acquires fast scans in the x-axis and slow scan in the y-axis, where y-axis movement artifacts are mostly generated from minor fixational eye movements such as drift, which are difficult to detect. Therefore, y-movement correction is not studied in this manuscript. A statistical model is used to estimate the misalignment of A-scans, instead of a transformation model between 2-D images. Independent A-scan features are extracted as common features for tracking. The approach is independent and does not rely on any reference images and overcomes most of the eye movement difficulties stated above.

II. METHOD

Particle filtering has been recognized as an effective target tracking algorithm due to its accuracy, robustness and flexibility in nonlinear and non-Gaussian systems [17]–[19]. The basic idea of particle filtering is to present the target by a state space model and convert the target tracking into a state estimation problem. The state at a given time in the dynamic system is estimated by its simulated probability density generated from a set of weighted samples, called particles (Fig. 2).

The spatial distortion in the 3-D OCT volume data is the combined effect of several eye movement factors. Moreover, the spatial variation between A-scans comes from natural anatomy as well. Particle filtering is a promising approach for statistical solution of a nonlinear alignment problem. Because of the intra-B-scan z-movement, each A-scan (1024

× 1 voxels) in the 3-D OCT image (200 × 200 × 1024 voxels) is considered as a processing unit instead of the 2-D patch in the B-scan. The proposed method is to track A-scan movement in the 3-D dataset. It is actually object tracking in one dimension, which causes more difficulties due to the lack of robust features for similarity measurements compared to 2-D object tracking in the general cases. Based on our results, the algorithm is more stable when correcting x- and z-axis movements separately rather than a one step xz-movement correction. Therefore, an x-movement correction is first performed by an implementation of a particle filtering algorithm, followed by z-movement correction. The kernels of particle filtering include state space, system dynamics, observations, and state estimation.

A. State Space

The 3-D OCT volume data generated from consecutive B-scans is considered as a dynamic system that is changing over time, represented by $\boldsymbol{X}_t$, where the first B-scan is set to be time $t = 0$. The state space is represented in the spatial domain as the 3-D location of an A-scan, donated by $\boldsymbol{X}_t\{\boldsymbol{a}_t(x, y, z)\}$. A number of A-scans are selected on the first B-scan ($t = 0$) as the initial states, denoted by

$$\boldsymbol{X}_0 \left\{ \boldsymbol{a}_0^1 (x, y, z), \boldsymbol{a}_0^2 (x, y, z) \cdots \boldsymbol{a}_0^M (x, y, z) \right\} \tag{1}$$

where M is the number of states in state space [Fig. 3(a)]. The initial states can be selected randomly or using a predefined distribution pattern. In this study, considering the computational efficiency in the 3-D OCT data, we attempted to use the majority of the B-scan without redundancy. Therefore, the spatial locations of a few equally spaced A-scans were used as the initial states. The state of the system (the locations of the selected A-scans) is updated frame by frame using particle filtering, in order to detect the eye movement.

A particle set is used to represent the state in a statistical model (i.e., probability density). For each state $\boldsymbol{a}_t^m (x, y, z)$, a set of weighted samples is generated as particles in the previous frame, denoted as

$$\boldsymbol{a}_{t-1}^m (x, y, z) \sim \left\{ w_{t-1}^{m,n}, \boldsymbol{s}_{t-1}^{m,n} (x, y, z) \right\}, n=1 \cdots N \tag{2}$$

where $\boldsymbol{s}_{t-1}^{m,n} (x, y, z)$ is the th particle of the th stateat time $t - 1$, and $w_{t-1}^{m,n}$ is the particle weight. Each sample consists of a particle that represents the hypothetical state and a corresponding discrete sampling probability w, where $\Sigma_{n=1}^{N} w_{t-1}^{m,n} = 1$. To deal with the abrupt x-axis movement, we use a Gaussian distribution to generate the particle set for each state in x-alignment. Uniform distribution is used to obtain particle set in z-alignment. Particles are predicted by a system dynamics model in the current frame [Fig. 3(b)]. An observation model is designed to compute the likelihood between each particle and the state in the previous frame, which is used to approximate the probability density of the state. The displacement of the state in the current frame is obtained by taking the expectation [Fig. 3(c)].

B. System Dynamics

System dynamics is used to predict the tendency of the object movement, which is computed by the previous states. A linear regressive model is chosen for the system dynamics between adjacent B-scans, written as

$$\boldsymbol{X}_t = A\boldsymbol{X}_{t-1} + B \tag{3}$$

where matrix A is initially set to an identity matrix and matrix B is set to a zero matrix. Two matrices are updated from two previous sequences $\boldsymbol{X}_{t-1}$ and $\boldsymbol{X}_{t-2}$.

C. Observation Model

The observation is defined as the similarity between the current particle and the state in the previous frame. To preprocess the image, a median filter is applied on each A-scan to smooth the A-scan profile and reduce the effect of speckle noise. A window-based similarity measurement is used to compute the observations of particle set at time t, written as

$$\boldsymbol{Y}_t\{\boldsymbol{y}_t^{m,n}\}, \boldsymbol{y}_t^{m,n}=\boldsymbol{H}\left(\boldsymbol{a}_{t-1}^{m}, \boldsymbol{s}_t^{m,n}\right) m=1\cdots M,\ n=1\cdots N \tag{4}$$

where $\boldsymbol{y}_t^{m,n}$ donates the observation of the nth particle for the mth state at time t, $H(\bullet)$ is a similarity measurement between the given particle at current frame (time t) and its corresponding state at previous frame (time $t-1$). In this paper, each A-scan is first converted into dozens of features, the similarity is computed based on the mean of absolute differences (SAD) between the candidate and reference window in the feature space.

The selection of reliable image features is essential to compute the observations and then calculate the probability density of the given state. For the x-alignment, common 2-D features are not reliable due to the intra-B-scan z-movement. Since 3-D OCT volume data is first aligned in the x direction, z direction independent features are extracted from each of the A-scans. For the z-alignment, the entire smoothed A-scan profile is used as features to compute the similarity.

The feature selection criteria in x-alignment are: 1) 1-D features (z direction) extracted from every single A-scan, 2) the features need to be independent to z-offset, 3) the features can enhance the local landmark between adjacent B-scans, such as blood vessel. There is an apparent difference between A-scan profiles with and without blood vessels, as shown in Fig. 4. This difference can be enhanced and summarized by a group of features to use in tracking. 1-D Haar-function filters with different window sizes are applied on each A-scan to generate A-scan features. We used two different 1-D Haar-features as shown in Fig. 5, where −1 and 1 regions have the same window size. The features taken are max, min, max-min, and zeroth to fourth central moments of the Haar-function filter responses. Other features including mean, standard deviation, skewness, and kurtosis, are also taken from each A-scan.

D. State Estimation

For each state at time t, $\boldsymbol{X}_t\{\boldsymbol{a}_t^m(x,y,z)\}, m=1\cdots M$, $m=1\cdots M$, a weighted particle set is generated in previous frame based on a Gaussian distribution and predicted in the current frame using a system dynamics model [Fig. 3(b)], written as

$$\boldsymbol{S}_t\left\{\left\{w_t^{1,n}, \boldsymbol{s}_t^{1,n}\right\}, \left\{w_t^{2,n}, \boldsymbol{s}_t^{2,n}\right\}\cdots\left\{w_t^{M,n}, \boldsymbol{s}_t^{M,n}\right\}\right\} \tag{5}$$

where N is the number of particles and is the particle weight, initially set to $1/N$ equally. In particle filtering, the state posterior distribution can be approximated by the observations of weighted particles, denoted as

$$p\left(\boldsymbol{X}_t\{\boldsymbol{a}_t^m\}|\boldsymbol{Y}_t\{\boldsymbol{y}_t^m\}\right)\sim\left\{w_t^{m,n}, \delta\left(\boldsymbol{s}_t^{m,n}\right)\right\}, n=1\cdots N \tag{6}$$

where $\delta(\bullet)$ is a Dirac delta function. The weights of particles $w_t^{m,n}$ are proportional to observations $y_t^{m,n}$ by computing the likelihood between the window of predicted location in

the current frame and thewindow of the state in previous frame. Particles' weights are normalized as $\Sigma_{n=1}^{N} w_t^{m,n} = 1$, which denote the discrete sampling probabilities of the corresponding particles. The displacement of each given state in current B-scan is obtained by estimating the functional state's expectation [Fig. 3(c)]

$$\widehat{Eg}(\boldsymbol{X}_t\{\boldsymbol{a}_t^m\}) = \sum_{n=1}^{N} w_t^{m,n}\delta(\boldsymbol{s}_t^{m,n}) \tag{7}$$

In this study, the state is updated by the weighted summation of particles with the top 10% largest weights.

E. X- and Z-Movement Estimation

For the x-movement estimation, state space is simply reduced to one dimension, denoted as $\boldsymbol{X}\{\boldsymbol{a}(x)\}$. Because the x-axis movement is perpendicular to the A-scan direction (z axis), each A-scan is first converted into dozens of z-independent features. The spatial locations of eleven equally spaced A-scans are set to the initial states to track A-scan misalignment in the x direction. The final x-axis movement of every single A-scan between adjacent B-scans is computed by a linear model using these eleven states in the current and previous frame, written as

$$\boldsymbol{a}_t(x) = \beta\boldsymbol{a}_{t-1}(x) + \gamma \tag{8}$$

where β and ρ are coefficients of a linear movement model, which are optimized using the least square method based on 11 states. Due to the changes of the states between adjacent B-scans, β and ρ and are different frame by frame. The x-axis movement is corrected by aligning the entire B-scan to the previous B-scan based on the linear models. This procedure can be performed within and outside the ONH, since the entire B-scan is aligned together.

After the x-axis movement is corrected, the same procedures are applied on the corrected 3-D data to estimate z-axis movement. The state space is reduced to one dimension in the z direction, notated as $\boldsymbol{X}_t\{\boldsymbol{a}_t(z)\}$, while feature space is set to the original A-scan intensity value. The spatial locations of sixteen equally spaced A-scans at $t = 0$ are set to the initial states. The z-axis movements of the given states are estimated based on the state updates in each frame, while z-axis movements between states are computed by 1-D interpolation.

In the z-alignment, the particle observation is computed based on each A-scan alone. Various shapes inside the ONH region may introduce errors in the similarity measurement of particle observation. In order to account for this potential problem, ONH margin is automatically detected on the OCT fundus image using the active contour model [20], and the particle filtering process is not performed within this region. Instead, 1-D interpolation is applied on each B-scan to estimate z-axis movement inside the ONH region.

III. SIMULATED DATA AND OBJECTIVE EVALUATION

A. Simulated Data

In order to test the performance of the algorithm, a series of 3-D OCT volume data with simulated eye movement artifacts were generated. Twenty-nine 3-D OCT images were selected for the simulation dataset (Cirrus HD-OCT, Optic disc cube 200 × 200 scan protocol). The image resolution is 200 × 200 × 1024 samplings in a cube of 6 × 6 × 2 mm. Images without observable x-axis movement artifacts on the OCT fundus image were selected. The simulation included only x-axis movements because z-axis movement artifacts

are generally caused by high frequency eye movement, which is unavoidable in real 3-D OCT volume data.

Various amplitudes of x-axis movements with the range of 2–10 pixels were simulated for each 3-D OCT image and corresponding spatial distorted 3-D dataset were generated. In the simulation operation, the x-axis movement was simplified to abrupt eye movements with three levels of amplitudes: small (2–4 pixels), medium (5–7 pixels), and large (8–10 pixels), as shown in Fig. 6. Only one x-axis movement artifact was introduced in each 3-D dataset at a random location and direction. The simulation was run inside and outside the optic nerve head (ONH) region separately to test the effect of the different retinal structure on the optic disc region.

B. Objective Evaluation

The accuracy (residual shift), sensitivity and specificity of x-movement correction were evaluated. The proposed algorithm was applied on each 3-D OCT volume data with simulated spatial distortion, to trace the amount of x-displacement frame by frame. The frame index with the simulated x-axis movement artifact was denoted as m. The detected amount of x-displacement at the frame m was compared with the simulated value to quantitatively evaluate the accuracy of the algorithm. The sensitivity of the algorithm for detecting movement and specificity for no-movement detection were computed without considering the amplitude of the movements.

C. Simulation Result

Table I summarizes the simulation result for the different eye movement amplitude levels inside and outside the ONH region. The average difference between the algorithm measured movement and the known simulated movement was 0.22 pixel (4.81%). The sensitivity and specificity of the x-movement detection were 98.85% and 99.43%, respectively. All the subgroup testing performed similarly as the overall result, except that the testing with small eye movement inside the ONH region had the largest residual shift and lowest sensitivity.

IV. EXPERIMENTAL DATA AND RESULT

A. Experimental Data

The algorithm was also tested on an independent dataset of 74 3-D OCT images centred on the optic disc, taken from 25 healthy and 49 glaucomatous eyes, using the same scanning protocol as described above. The inclusion criteria for this dataset require the presence of clearly observable z-axis movement, blood vessel discontinuities, and/or optic disc distortions. This dataset represents the real-life clinical situation where acquired images often contain eye movement artifacts. Particle filtering was applied on each 3-D OCT image. The entire processing with MATLAB, including generation of the corrected 3-D data, and saving the results on a hard disk, lasted approximately 7 min.

B. Subjective Evaluation

The algorithm was subjectively evaluated by comparing the processed and original 3-D OCT images side by side. Each processed image was evaluated with respect to overall x-movement correction and z-movement correction. Assessment of x-axis correction was based on the global blood vessel continuity on the OCT fundus image. The retinal pigment epithelium [RPE, Fig. 7(a) and (b)] layer of the retina is typically flat within 6 × 6 mm OCT scan region. Therefore, overall z-correction considered whether RPE layer was flat or not on the horizontal and vertical center B-scans generated from 3-D OCT volume data. The results were labeled as improved, equivalent, and degraded.

C. Experimental Result

Particle filtering was applied on the 3-D OCT volume data frame by frame to correct x-axis movement and then z-axis movement. The overall 3-D OCT correction took 7 min using MATLAB (Mac OS X 10.6.8, 2.4-GHz Intel Core 2 Duo, and 2-GB 667-MHz DDR2 SDRAM). Examples of the results of particle filtering based 3-D OCT alignment is given in Fig. 7. Two original 3-D OCT volume data with spatial distortions are illustrated in Fig. 7(a). Blood vessel discontinuity generated by micro-saccades could be observed on their OCT fundus images [Fig. 7(c)]. The z-axis movements generated from fore–aft eye movements are shown in their vertical OCT B-scans [Fig. 7(e)]. The particle filtering approach efficiently corrected micro-saccades and z-axis movements by aligning B-scans and A-scans. The corrected 3-D OCT volume data and their corresponding OCT fundus images and vertical B-scans are shown in Fig. 7(b), (d), (f). Table II gives the subjective evaluation of the processed images with respect to x- and z-movement corrections. All the images were improved after z-alignment, while 81.1% images were improved after x-alignment.

V. DISCUSSION

The main difficulties of 3-D OCT eye movement correction are the complicate nature of eye movement and the lack of reference. The proposed algorithm used intrinsic features to align A-scans in the 3-D dataset. It did not rely on any reference image or additional scan. A-scan alignment only used 1-D A-scan features but not 2-D B-scan features. Therefore, z-axis movements within a B-scan did not affect the alignment processing. Another advantage of this method is the use of a statistical model to estimate the A-scan movement, which could handle various types of eye movements and their combinations. Therefore, it was not necessary to design a particular movement model for each type of eye movement.

To reduce the redundancy and have a more efficient computation, the proposed A-scan tracking algorithm is initiated from a few A-scans with equal interval in the first B-scan in the image. The overall 3-D OCT image alignment took approximately 7 min using MATLAB, which is an acceptable processing time in real-time clinical utility. Dedicated programming may substantially shorten this duration. For x-movement correction, some particular A-scans, such as A-scans with blood vessels, may provide more robust tracking results due to their differences from neighboring samplings. However, the blood vessel approach is only suitable for locations with apparent vessel network, but will be of limited use in locations deprived of major blood vessels such as the macular region. Further studies are warranted to explore this method.

In Table I, we computed “residual shift,” “sensitivity,” and “specificity” to objectively evaluate the algorithm performance with the simulated data. “Residual shift” measures the absolute difference of the movement amplitude compared with the reference, thus quantitatively evaluating the accuracy of the algorithm. “Sensitivity” and “specificity” measure the ability of identifying movement and no-movement regardless of amplitude.

Although good quality OCT images were carefully selected as ideal images for the simulated data, it is possible to have some small invisible eye movement artifacts in the data. Moreover, it was still unavoidable to have z-axis movement artifacts in each single 3-D OCT dataset when real eyes were scanned. Therefore, the performance of z-alignment was not evaluated with the simulated data in this study. Scanning a model eye could solve this problem and obtain motion-free images in all directions.

The proposed algorithm aligned 3-D datasets without using any reference image or scan. It is based on the assumption that adjacent A-scans share common features. However, the A-

scan alignment may introduce artifacts in 3-D OCT data [Fig. 7(D2)]. Testing various eye movement amplitudes and locations on the simulated data, the software had the largest residual shift and lowest sensitivity on the subgroup with small eye movement inside the ONH region. This might be explained by the different anatomical features in the ONH compared to the region surrounding it that makes it difficult to distinguish small misalignments but relatively easy to introduce artifacts. Separating the true eye movement and the software introduced artifacts will be studied in the future.

The advantage of the proposed method is that it does not need any reference and only uses one 3-D OCT scan to correct the eye movement. However, the limitation of the current status of this technology is that y-movement cannot be detected due to the current OCT scan pattern with fast scan in x-axis and slow scan in y-axis. This method was designed to address a fundamental need in clinical practice, i.e., the OCT images that had been acquired at each visit had motion artifacts and the patient had completed their appointment and left. To longitudinally monitor the pathological changes of the eye, all previous scans at each visit are needed. Therefore, it is important to design a method to process the existing dataset to improve the image quality, i.e., the spatial integrity of the 3-D data. The straightforward method is to use one or several external reference images to correct the eye movement artifacts to obtain the spatial integrity restored 3-D data. However, the external reference was not always available in the existing dataset. The proposed method is able to correct the eye movement in x and z directions without using any reference. Although the proposed method cannot fix all kinds of movement in the 3-D dataset, it enhances the image quality, improves the reliability, and turns some previously not clinically useful images into useful images. This has significant impact on the longitudinal study to monitor the structural changes and disease progression.

The problem of y-movement can be solved by including an additional 3-D OCT scan with orthogonal fast scan axis [15] or an external 2-D reference image [7], [8]. However, for the former solution, currently commercial OCT devices do not provide the scan protocol of two 3-D cube scans with orthogonal fast scan axis. For the latter solution, only x- and y-axis eye movements are corrected. To correct the eye movement in any situation, a more flexible and feasible solution is to utilize a two-tiered approach: 1) correction without external reference image, and 2) correction with external reference image. Our proposed particle filtering method can be used as the first step to correct the x- and z-axis eye movements, in order to improve the image quality for the images without any reference. In the second step, combining with an available reference image, the eye movements in all three directions can be corrected by registering the x- and z-aligned 3-D OCT data on the external reference image to correct y-movement and rotational movement. This two-tiered approach will be investigated in the future to achieve the goal of correcting the 3-D OCT eye movement in all three directions.

VI. CONCLUSION

We presented a particle filtering approach for automatic alignment of 3-D OCT volume data in x- and z-directions. The algorithm does not rely on any reference image or scan. Experimental results show the proposed algorithm is an efficient method to correct eye movement and provide spatial integrity restored 3-D OCT data, which is an essential foundation of the quantitative OCT analysis.

Acknowledgments

This work was supported in part by the National Institutes of Health (NIH) under Grant NIH R01-EY013178 and Grant P30-EY008098, in part by the Eye and Ear Foundation (Pittsburgh, PA), and in part by Research to Prevent Blindness.

REFERENCES

[1]. Schuman JS. Spectral domain optical coherence tomography for glaucoma. Trans. Am. Ophthalmol. Soc. 2008; vol. 106:426–428. [PubMed: 19277249]

[2]. Picard Y, Thompson C. Motion correction of PET images using multiple acquisition frames. IEEE Trans. Med. Imag. Apr.1997 vol. 16(no. 2):137–144.

[3]. Fulton R, Meikle S, Eberl S, Pfeiffer J, Constable C, Fulham M. Correction for head movements in positron emission tomography using an optical motion-tracking system. IEEE Trans. Nucl. Sci. Feb.2002 vol. 49(no. 1):116–123.

[4]. Buhler P, Just U, Will E, Kotzerke J, Hoff J. An accurate method for correction of head movement in PET. IEEE Trans. Med. Imag. Sep.2004 vol. 23(no. 9):1176–1185.

[5]. Yu CL, Huang SC, Dahlbom M, Bergsneider M. Alignment of transmission and emission scans of PET to correct for subject movement using a sinogram consistency criterion. Proc. 2003 IEEE Nucl. Sci. Symp. Conf. Rec. Oct.2003 vol. 4:2889–2892.

[6]. Liao R, Krolik J, McKeown MJ. Movement correction of fMRI time-series using intrinsic statistical properties of images: An independent component analysis approach. Proc. 2002 IEEE Int. Symp. Biomed. Imag. 2002:765–768.

[7]. Ricco S, Chen M, Ishikawa H, Wollstein G, Schuman JS. Correcting motion artifacts in retinal spectral domain optical coherence tomography via image registration. Proc. Med. Imag. Computing Computer Assist. Intervent. (MICCAI). Sep.2009 :100–107.

[8]. Xu, J.; Ishikawa, H.; Tolliver, DA.; Wollstein, G.; Miller, GL.; Bilonick, RA.; Kagemann, L.; Schuman, JS. Shape context algorithm applied to correct eye movement artifacts on three-dimensional (3-D) spectral domain optical coherence tomography (SD-OCT). presented at the Reducing Disparities in Eye Disease and Treatment, 2009 ARVO Annu. Meeting; Ft. Lauderdale, FL. May 2009;

[9]. Goshtasby, A. Ardeshir 2-D and 3-D Image Registration: For Medical, Remote Sensing, and Industrial Applications. Wiley; New York: 2005.

[10]. [Online]. Available: http://www.heidelbergengineering.com/products/spectralis-hra-oct/

[11]. [Online]. Available: http://www.meditec.zeiss.com/cirrus

[12]. Belongie S, Malik J, Puzicha J. Shape matching and object recognition using shape context. IEEE Trans. Pattern Anal. Mach. Intell. Apr.2002 vol. 24(no. 4):509–522.

[13]. Xu J, Tolliver D, Ishikawa H, Wollstein G, Schuman JS. 3-D OCT retinal vessel segmentation based on boosting learning. World Congress Med. Phys. Biomed. Eng. 2009; vol. 25:179–182.

[14]. Xu J, Ishikawa H, Wollstein G, Schuman JS. Retinal vessel segmentation on SLO image. Proc. IEEE Eng. Med. Biol. Soc. Sep.2008 :2258–2261.

[15]. Kraus, M.; Mayer, MA.; Bock, R.; Potsaid, B.; Manjunath, V.; Duker, JS.; Hornegger, J.; Fujimoto, JG. Combination of multiple motion corrected OCT volume scans for noise reduction and extraction of arbitrary cross-sectional images. presented at the 2010 ARVO/ISIE Imag. Conf.; Ft. Lauderdale, FL. May 2010;

[16]. Antony B, Abràmoff MD, Tang L, Ramdas WD, Vingerling JR, Jansonius NM, Lee K, Kwon YH, Sonka M, Garvin MK. Automated 3-D method for the correction of axial artifacts in spectral-domain optical coherence tomography images. Biomed. Opt. Express. Aug.2011 vol. 2(no. 8):2403–2416. [PubMed: 21833377]

[17]. Yan Z, Yeary MB, Cheng S, Kehtarnavaz N. An object-tracking algorithm based on multiple-model particle filtering with state partitioning. IEEE Trans. Instrum. Meas. Apr.2009 vol. 58(no. 5):1797–1809.

[18]. Doucet, A.; Johansen, AM. A tutorial on particle filtering and smoothing: Fifteen years. Dept. Stat., Univ. British Columbia; Vancouver, BC, Canada: Tech. Rep.

[19]. Xu J, Ishikawa H, Wollstein G, Schuman JS. 3-D OCT eye movement correction based on particle filtering. Proc. IEEE Eng. Med. Biol. Soc. Sep.2010 :53–56.

[20]. Xu J, Ishikawa H, Wollstein G, Bilonick RA, Sung KR, Kagemann L, Schuman JS. Automated assessment of optic nerve head on stereo disc photographs. Invest. Ophthalmol. Vis. Sci. 2008; vol. 49:2512–2517. [PubMed: 18326698]

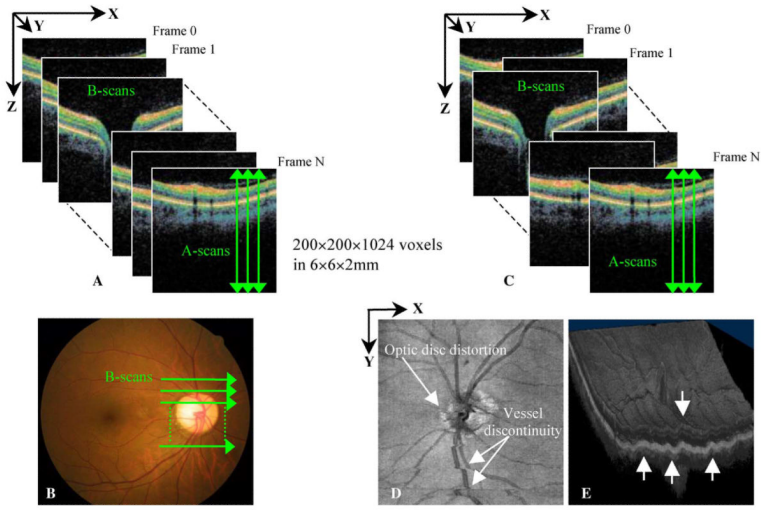

Fig. 1.

Example of a 3-D OCT image. (a) 3-D OCT image composed of consecutive B-scans, each B-scan consists of a certain number of A-scans. (b) Corresponding scanning region on fundus photograph. (c) 3-D OCT image with eye movement. (d) OCT fundus image, generated by averaging intensity values of each A-scan. The blood vessel discontinuity and optic disc distortion are illustrated. (e) 3-D OCT volume data with z-movement (arrows).

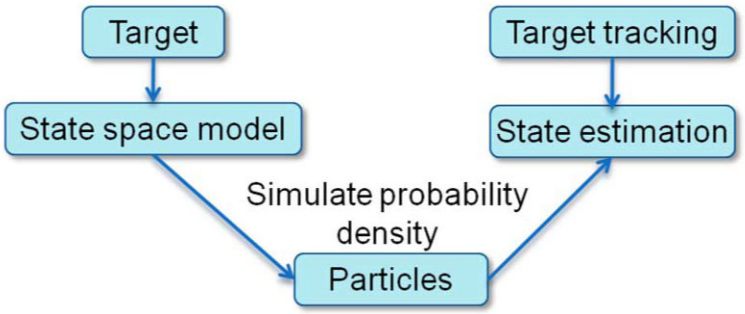

Fig. 2.
Target tracking based on particle filtering.

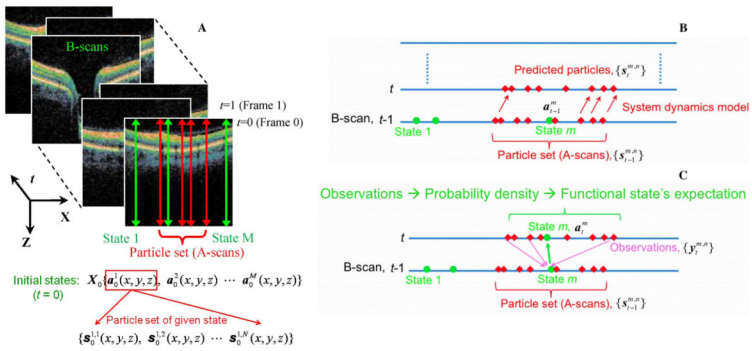

Fig. 3.

Concepts of particle filtering. (a) State space and particle set. (b) System dynamics. (c) Observations and state estimation.

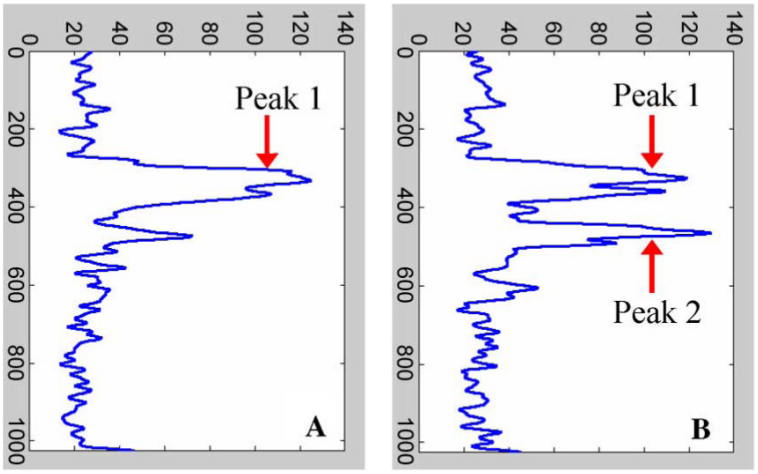

Fig. 4.

Examples of smoothed vessel A-scan profile (a) and non-vessel A-scan profile (b). There are typically two primary peaks in non-vessel A-scan profile corresponding to retinal nerve fiber layer and retinal pigment epithelium layer, while only one peak can be observed in vessel A-scan profile due to the blood vessel shadow.

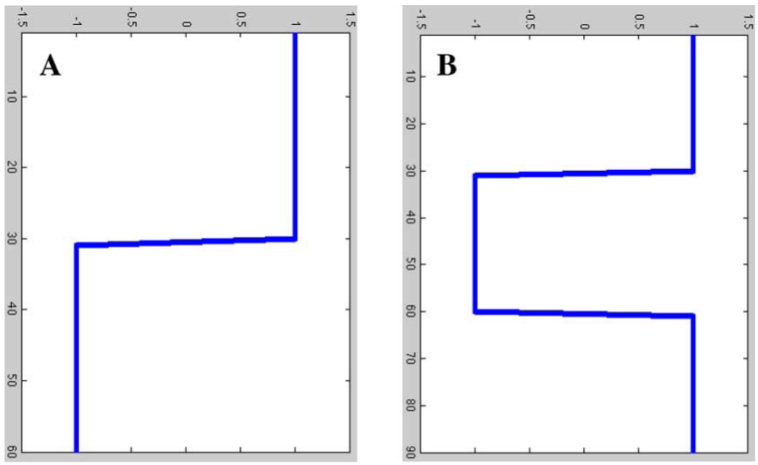

Fig. 5.
1-D Haar-feature filter. (a) two-window Haar-feature, (b) three-window Haar-feature.

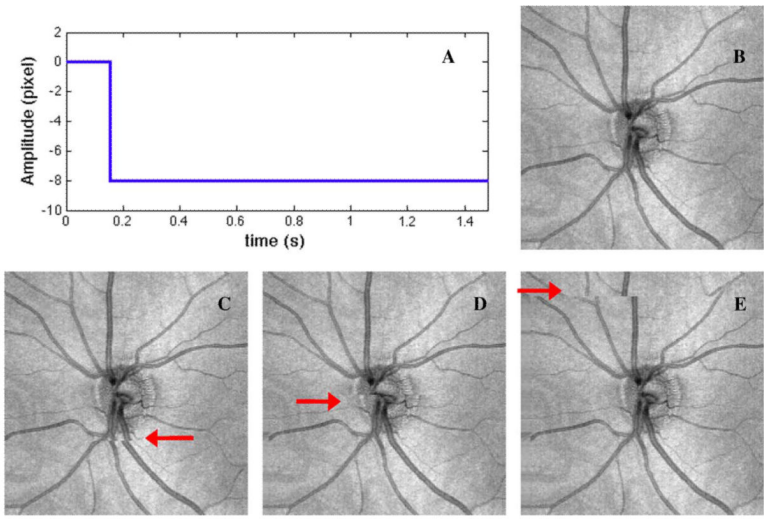

Fig. 6.

Simulated eye movement artifacts. (a) Abrupt eye movement in x direction, with eight pixel amplitude in the right direction. (b) OCT fundus image without any x-movement. (c) Three pixel x-movement (small) at the 140th frame moving to left. (d) Five pixel x-movement (medium) at the 102nd frame inside ONH region moving to right. (e) Eight pixel x-movement (large) at the 21st frame moving to right.

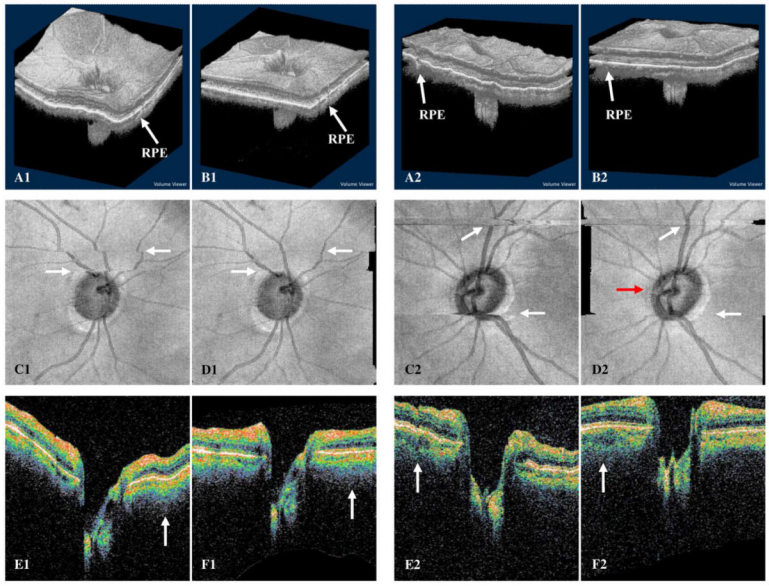

Fig. 7.

Two examples of 3-D OCT eye movement correction using particle filtering. (A1, 2) 3-D OCT volume data with eye movements. (B1, 2) Corrected 3-D OCT volume data. (C1, 2) OCT fundus images with blood discontinuity caused by eye movements. (D1, 2) Corrected OCT fundus images. Note the appearance of algorithm generated artifact in ONH region labeled with red arrow (D2). (E1, 2) Vertical OCT B-scans with z-axis eye movement artifacts. (F1, 2) Corrected vertical B-scans.

TABLE I

Quantitative Evaluation of the Proposed Eye Movement Correction Algorithm Using Simulated Data

Simulated eye movement amplitude	Residual shift in pixel (percentage)	Sensitivity	Specificity
Overall	0.22 (4.81%)	98.85%	99.43%
Small, outside ONH	0.07 (1.72%)	100%	99.42%
Medium, outside ONH	0.38 (6.62%)	100%	99.48%
Large, outside ONH	0.17(1.81%)	100%	99.45%
Small, inside ONH	0.31 (12.93%)	93.10%	99.44%
Medium inside ONH	0.21 (3.60%)	100%	99.45%
Large, inside ONH	0.21 (2.18%)	100%	99.39%

ONH—optic nerve head, overall—2–10 pixels including both inside and outside ONH region, small—2–4 pixels, medium—5–7 pixels, large—8–10 pixels.

TABLE II

Subjective Evaluation of 74 Processed 3-D OCT Images

	Grade	Evaluation
X-movement correction	Improved	60 (81.1%)
	Equivalent	13(17.6%)
	Degraded	1 (1.4)%
Z-movement correction	Improved	74(100%)
	Equivalent	0 (0%)
	Degraded	0 (0%)